J Therm Anal Calorim (2015) 119:1191–1198
DOI 10.1007/s10973-014-4223-3

Specific heat and magnetocaloric effect studies in multiferroic $YMnO_3$

N. Kumar Swamy · N. Pavan Kumar · P. Venugopal Reddy · Manish Gupta · S. Shanmukharao Samatham · D. Venkateshwarulu · V. Ganesan · Vikas Malik · B. K. Das

Received: 17 January 2014 / Accepted: 27 September 2014 / Published online: 16 October 2014

Abstract Multiferroic bulk $YMnO_3$ sample was prepared through the solid state reaction method. After characterizing the sample structurally, a systematic investigation of magnetization and specific heat has been undertaken over a temperature range 2–300 K under different magnetic fields. Based on these studies, it has been found that the sample exhibited a paramagnetic to ferrimagnetic phase transition of spin glass type at $\sim$42 K that could be attributed to spin cantering. The magnetic transition peak seen in the magnetic entropy change versus temperature curves became broader with increasing magnetic field. A large magnetic entropy change of $\sim$1 J mol^{-1} K^{-1} was obtained under a magnetic field change of 0–10 T.

Keywords Multiferroics · Specific heat (C_p) · Magnetocaloric effect · Manganite

N. Kumar Swamy · M. Gupta · V. Malik · B. K. Das
Material Science Research Lab, ITM University, HUDA Sector 23A, Gurgaon 122017, Haryana, India

N. Kumar Swamy (✉)
School of Engineering and Research, ITM University, Uparwara, New Raipur 493661, CG, India
e-mail: nkumarswamy15@gmail.com

N. Pavan Kumar · P. V. Reddy
Department of Physics, Osmania University, Hyderabad 500007, A.P., India

S. S. Samatham · D. Venkateshwarulu · V. Ganesan
Low Temperature Lab, UGC-DAE CSR, DAVV Campus, Khandawa Road, Indore 452017, M.P., India

V. Malik
School of Physical Sciences and Material Science, Jaypee Institute of Information Technology, Noida 201301, U.P., India

Introduction

The multiferroic materials are materials that simultaneously show more than one second-order transition phenomena such as ferroelectricity and ferro/antiferromagnetism and ferroelasticity. If the ordering phenomena are coupled, one type of ordering can influence the parameters of other type of ordering leading to practical applications. For example, if the ferroelectricity can be coupled to ferromagnetism, dielectric properties can be controlled by the application of magnetic fields or the magnetic properties can be controlled by application of electric fields. Although the mechanisms for second-order ferroelectric and magnetic ordering phenomena are very similar in many ways, their coexistence in the same material is infrequent. Rare-earth manganite ($RMnO_3$) compounds (R represents Y and rare-earth ions from Ho to Lu) have been found to show such coexistence of ferroelectricity and ferro/antiferromagnetism in them. In these compounds with hexagonal or orthorhombic crystal structure (i.e., distorted perovskite structure), the spin–spin interactions between Mn^{3+} ions present within their close-packed basal planes are dominant [1–7]. Rare-earth manganites with different rare-earth ions present at the rare-earth sites show different magnetic phases ranging from ferromagnetic-to-ferrimagnetic-to-antiferromagnetic-to paramagnetic [3, 5, 6] and consequently exhibit different physical properties below their magnetic transition temperature. Among the rare-earth manganites with hexagonal crystal structure, $YMnO_3$ is relatively simple because a single magnetic sublattice of Mn is present and the material has been investigated by several authors [8, 9]. Below 1000 K, they undergo a paraelectric-to-ferroelectric transition to a non-centrosymmetric structure with the space group $P6_3cm$ [9]. At lower temperatures near 100 K, these manganites order with a non-collinear antiferromagnetic structure.

For technological applications in low temperatures like refrigeration for liquefaction of hydrogen and rocket engines [10–14], materials showing large magnetocaloric effect are important. Study of magnetocaloric effect also leads to better understanding the low temperature magnetism and physics of magnetic refrigeration. $RMnO_3$ materials also show large magnetocaloric effect. However, their practical applications in magnetic refrigeration have not been investigated yet. Here we report the magnetocaloric properties of bulk $YMnO_3$ calculated from specific heat measurements.

Experimental

Polycrystalline bulk $YMnO_3$ sample was prepared by the standard solid-state ceramic route. Considering the hygroscopic nature of the rare-earth material Y_2O_3 and MnO_2, they were given a pre-heat treatment at 1,000 °C for 10 h. The starting materials (of AR grade purity) were taken in the required stoichiometric ratio and were mixed by grinding in a mortar and pestle for five hours. The mixed powdered sample was twice calcined at 1,000 °C for 12 h in air ambient with an intermediate grinding. The calcined powder was subsequently pelletized and the pellets were sintered at 1,350 °C for 24 h in air ambient. The room temperature XRD patterns were recorded using a Rigaku Dmax 300 diffractometer using the CuK_α radiation. For microstructural analysis of the sample, a scanning electron microscope (SEM) of ZEISS EVO Series make (Model EVO 50) was used. Magnetization measurements (M-T) were carried out with a SQUID magnetometer (make MPMS XL) under field-cooled (FC) and zero-field-cooled (ZFC) protocols at an applied magnetic field (H) of 0.1 T. Magnetization (M-H) values were measured up to a maximum applied field (H) of 1–2 T at temperatures of 10, 30, and 50 K. Specific heat (C_p) measurements were carried out using a PPMS system at various applied magnetic fields in the temperature range 2–300 K.

Results and discussion

Structural characterization

The measured XRD powder diffraction pattern of $YMnO_3$ is shown in Fig. 1a. The Rietveld refinement technique was used to analyze the XRD data assuming $YMnO_3$ to have a hexagonal structure with $P6_3cm$ space group. XRD peak profiles were calculated using a pseudo-voigt function. Figure 1b shows the calculated Rietveld refined XRD patterns of the sample along with difference in the calculated and measured XRD diffraction patterns. The crystallographic data obtained

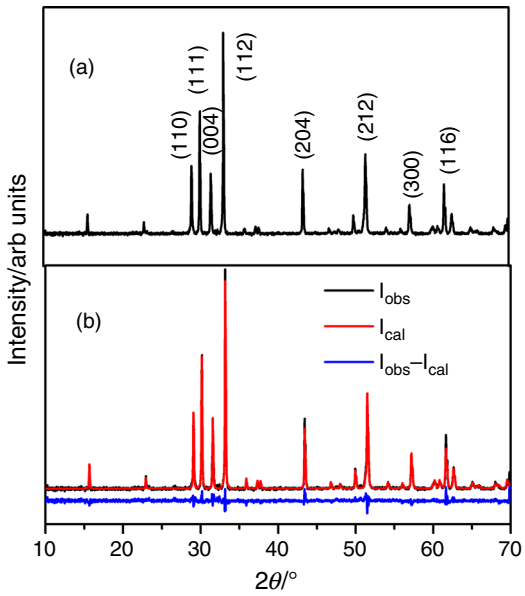

Fig. 1 X–ray diffraction measurement of $YMnO_3$ using Rietveld refinement technique assuming hexagonal structure with $P6_3cm$ space group—**a** gives the observed XRD peak intensities and **b** gives the calculated XRD peak intensities from the known structure for $YMnO_3$ and the differences between the observed and calculated values

from this analysis is given in Table 1. Figure 2 shows the SEM micrograph of the fractured surface of the $YMnO_3$ sample. From that figure, it could be concluded that all the grains were uniform and ~1.5 μm in size.

Magnetization measurement

Results of measurements of dc magnetization versus temperature (M-T) performed with application of an external magnetic field (H) of 0.1 T under temperature-dependent zero-field-cooled (ZFC) and field-cooled (FC) protocols are shown in Fig. 3. Temperature-dependent ZFC and FC magnetization values (Fig. 3) showed bifurcation between them at the temperature ~50 K. The ZFC curve displayed a sharp peak at around 42 K, where the irreversibility between ZFC and FC curves became obvious. Such a feature is the hallmark of a spin glass transition. A small amount of excess Mn present in $YMnO_3$ causing a deviation in stoichiometry can bring about the formation of a spin glass state [15]. In contrast to this, there are reports [9, 16] that there is no difference in the ZFC and FC curves of pure $YMnO_3$. However, alternately spin cantering at Mn^{3+} sites might also happen at low temperature leading to a spin glass like transition. Therefore, for $YMnO_3$ samples cooled under ZFC protocol, it was concluded that for the magnetic force applied later on would not be capable of aligning the spins aligned in random directions due to the viscous behavior of

Table 1 Lattice parameters and magnetic constants from XRD and magnetic susceptibility data

a/nm	b/nm	c/nm	R_p	R_{wp}	R_{exp}	GOF	C/cm^3 K mol^{-1}	Θ_N/K	μ_{calc}/μ_B	μ_{obs}/μ_B
0.6148	0.6148	0.1134	5.39	7.49	3.9	1.9	3.763	227	4.97	5.48

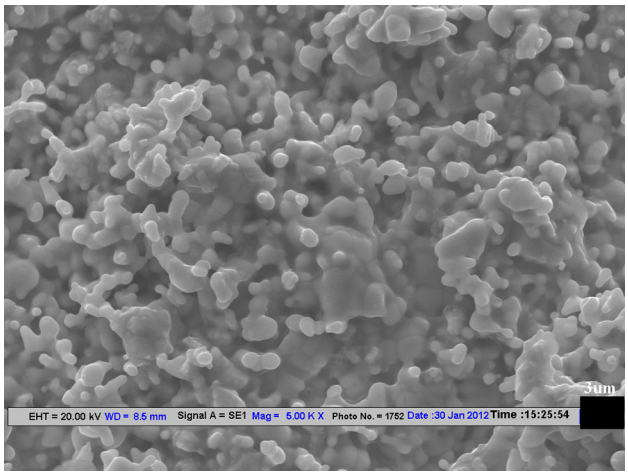

Fig. 2 SEM micrograph of fractured surface of $YMnO_3$ showing uniform grain size throughout the sample. The *black bar* at the right bottom corner measures 3 μm in length

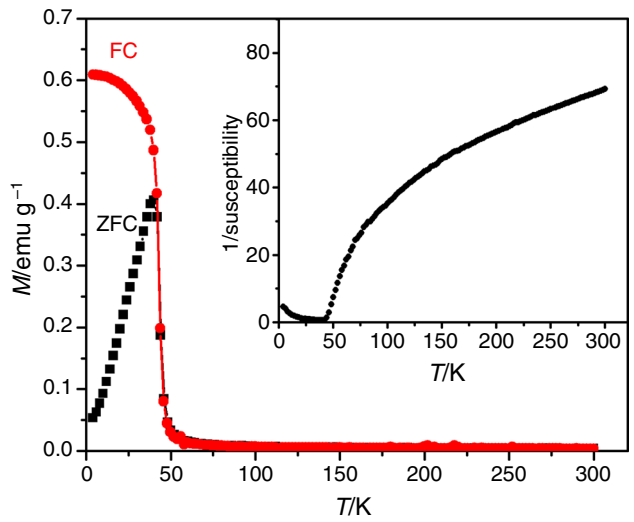

Fig. 3 ZFC-FC measurement of magnetization (M) at an applied magnetic field of 0.1 T versus temperature (T) for $YMnO_3$ showing divergence of the FC and ZFC curves below a temperature (called irreversibility temperature) of ~42 K. There is a clear indication and signature of a spin glass transition

the spins. High applied magnetic fields during FC protocol could align the spin cantering and hence would become responsible for a higher magnetic moment under FC protocol.

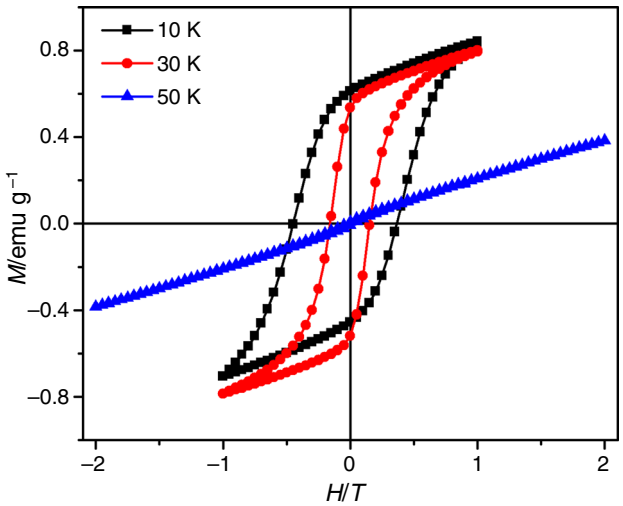

Fig. 4 Variation of magnetization (M) with applied magnetic field (H) curve for $YMnO_3$ up to a maximum applied magnetic field of 1–2 T at the temperatures of 10, 30, and 50 K showing M-H loops with hysteresis due to ferrimagnetic behavior at 10 and 30 K, but M-H loop at 50 K showing a mixed phase with both ferrimagnetic and paramagnetic phases present

Table 2 Parameter extracted from M-H measurements

$YMnO_3$	10 K	30 K	50 K
$n_B/\mu_B(2YMnO_3)^{-1}$	0.0562	0.05468	0.0264
$\alpha_{Y\text{-}K}$/degrees	13.6	13.4	9.312
H_c/Oe	4502.71	1577.51	932.28
M_R/emu g^{-1}	0.61241	0.53645	0.01487
M_s/emu g^{-1}	0.82027	0.7962	0.3843

For understanding of the nature of magnetic transition of the $YMnO_3$ sample, inverse of magnetic susceptibility (χ^{-1}) was plotted against temperature (T). High temperature (>150 K) M-T data could be fitted to the Curie law $\chi = C/(T + \Theta_N)$ consistent with the paramagnetic (PM) to antiferromagnetic transition (AFM) and the results are shown in the inset of Fig. 3. From the fittings, Neel temperature (Θ_N), Curie constant (C), and effective paramagnetic moment (μ) in Bohr magnetons (μ_B) have been obtained and are given in Table 1. Low temperature M-T data (Fig. 3) showed a spin glass transition with irreversibility temperature around 42 K that was consistent with observations of Chen et al. [15].

To understand the low temperature transition, M-H measurements were carried out below the transition

temperature of 42 K. Figure 4 shows the results of M-H measurements done on $YMnO_3$ below the spin glass transition at temperatures of 10, 30, and 50 K. These measurements showed hysteresis in M-H loops at temperature below 30 K. Remanence (M_R), coercivity (H_c), and saturation magnetization (M_s) were calculated and are shown in Table 2.

It was interesting to see that at temperatures less than 50 K, M-H measurement showed a ferrimagnetic behavior with a low value of saturation magnetization, M_s and at a temperature of 50 K, it showed a mixed phase consisting of both PM and ferrimagnetic phases. It can be concluded that a phase change from PM to ferrimagnetic occurred at a temperature below 50 K in $YMnO_3$. In the $YMnO_3$ sample, since the magnetic contribution is from Mn^{3+} ions at B-sites, and since Mn^{3+} ions would normally have anti-parallel alignment of their magnetic moments due to the B-B interaction, only possible magnetic interaction that could explain for the M-H curves at the low temperature in ferrimagnetic $YMnO_3$ could be arising only from cantering of spins of Mn^{3+} ions at B-sites.The cantering of the spins giving rise to Y-K angle (α_{y-k}), were calculated at 10 , 30 , and 50 K for $YMnO_3$ using the formula [17, 18]

$$n_B = M_B(x)(1 - \cos\ \alpha_{y-k}), \quad (1)$$

where M_B is the magnetization of Mn^{3+} ion and n_B, is the number of Bohr magneton per two $YMnO_3$ molecules and it has been calculated using the relation [19]

$$n_B = \frac{2MM_s}{N_A\mu_B}, \quad (2)$$

where M = molecular weight of $YMnO_3$, M_s = saturation magnetization, N_A = Avogadro's number.

The values of α_{Y-K} and n_B for $YMnO_3$ samples at temperature 10, 30, and 50 K are shown in Table 2. It was observed that the saturation magnetization (M_s) and magnetic moment per two $YMnO_3$ molecules, n_B, decreased with the temperature. The decrease in the α_{y-k} angles with increasing temperature may be attributed to the presence of triangular spin arrangement on B-site [17, 20]. This would lead to the reduction in the B-B exchange interaction and a consequent decrease in M_s.

Specific heat

Figure 5 shows the variation of specific heat (C_p) of $YMnO_3$ sample with temperature (T) under different magnetic fields (H). The specific heat increased with increase in temperature. It can be seen from figure that there was a clear transition at 42 K. This is the hallmark of a spin glass transition. These results are agreement with the magnetization results. The peak that appeared at 42 K in

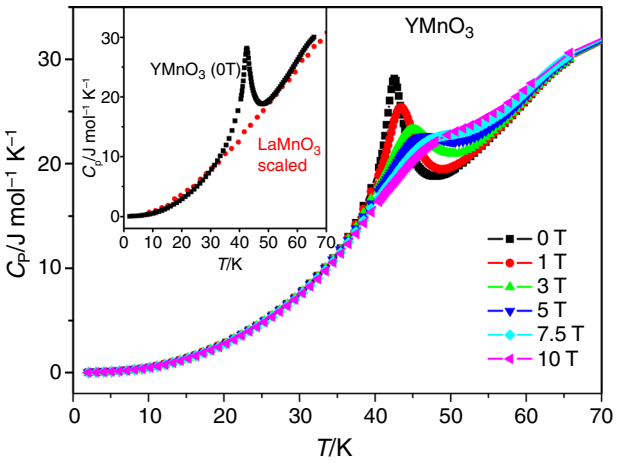

Fig. 5 Specific heat (C_p) of the $YMnO_3$ sample with temperature (T) under different magnetic fields. Peak was attributed to spin glass transition and peak broadening was due to ferrimagnetic ordering/cantering of spins. *Inset* shows how the magnetic contribution to the specific heat (C_M) was estimated by taking the lattice specific heat of $LaMnO_3$ from literature [26] and scaling it to fit the $YMnO_3$ data to obtain lattice specific heat of $YMnO_3$ and then taking the difference between the measured C_p and lattice specific heat as C_M

zero magnetic fields got smeared in the magnetic fields and gradually vanished at 10 T. The peak shifted to higher temperatures with wider spreads as the applied magnetic field increased. In fact, this is the primary signature of a ferromagnetic (or ferrimagnetic) material. Kimura et al. [21] also observed similar kind of behavior of the magnetic field dependent peak broadening in specific heat versus temperature data observed for some ferromagnetic materials [22] near the ferromagnetic transition temperature, which was verified from the M-H curves taken below and above the transition temperature. Tomuta et al. [23] suggested that such hump is due to system progressively searching for its true ground state, which can be verified by M-H and M-T graphs showing a constant increase in the susceptibility below the transition.

Magnetocaloric effect

Magnetocaloric effect (MCE) is studied for examining the possibility of refrigeration by changing the applied magnetic field. Some of the materials examined for their magnetocaloric properties are bulk and/or nanocrystalline $Gd_5(Si_2Ge_2)$ [24], γ-Fe_2O_3 [25], samarium ferrite [25], gadolinium ferrite [25], $PrMnO_3$ [26], Ca-doped $LaMnO_3$ [27], and Sr-doped $LaMnCoO_3$ [28]. The methods to study MCE can be divided into two methods—direct method and indirect method. In the direct method, the material is subjected to a magnetic field change and its change of temperature is directly measured by

different techniques [29]. In the indirect method, the parameters of MCE are determined from the magnetization and/or heat capacity data.

Experimental data of magnetization (M) versus applied magnetic field (H) can be used to calculate magnetic entropy change (ΔS_M) by using the equation:

$$\Delta S_M = \int_{H1}^{H2} \left(\frac{\partial M}{\partial H}\right) dH \quad (3)$$

The C_p versus T data measured in different magnetic fields also allows calculation of a complete set of parameters required for magnetic refrigerator design as discussed below. In order to calculate these parameters, entropy is calculated from the specific heat data using the formula given below:

$$S(T,H) = \int_{0}^{T} \left(\frac{C_p}{T}\right) dT. \quad (4)$$

Figure 5 shows the variation of specific heat of our bulk $YMnO_3$ with temperature at different magnetic fields. However, both lattice vibrations and magnetic field changes contributed to the measured specific heat and entropy. The lattice contribution to the specific heat (C_{lat}) was estimated from the C_{lat} values for non-magnetic $LaMnO_3$. For this purpose, the specific heat values were taken from the C_{lat} data of Cheng et al. [26]. To accommodate the difference in lattice contribution for the two different rare-earth compounds, it was assumed that specific heat follows a scaling law. According to this law, the lattice specific heat of a rare-earth compound follows the universal curve if plotted as a function of (T/T_R), where T_R is characteristic temperature of the compound. This assumption is similar to Debye or Einstein model where lattice specific heat of any material is represented by a single curve if T_R is Debye or Einstein temperature. Therefore, specific heat of La compound was made to overlap with that of $YMnO_3$ sample of the present investigation above the magnetic transition temperature (or in the PM region) by multiplying the C_p axis for $LaMnO_3$ with a suitable factor as shown in the inset of Fig. 5. The magnetic contribution to the specific heat (C_M) in the presence of external magnetic fields and consequent magnetic entropy (S_M) were calculated using the formula given below.

$$C_M = C_p - C_{lat} \quad (5)$$

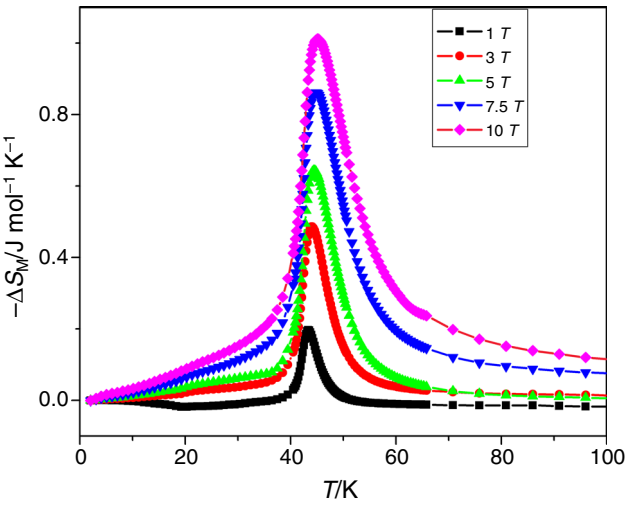

Fig. 6 This displays the magnetic contribution to the entropy change ($-\Delta S_M$) of $YMnO_3$ as a function of temperature (T) for various applied magnetic fields. Peaks can be seen near the transition temperature of ~42 K with temperature of the peak position shifting to higher temperatures and peak height increasing on increasing the applied magnetic field (H)

$$S_M(H) = \int_{0}^{T} \left(\frac{C_p - C_{lat}}{T}\right) dT \quad (6)$$

The change in magnetic contribution to entropy, ΔS_M, on application of a magnetic field, H, could be calculated as follows:

$$\Delta S_M = S(H) - S(0) \quad (7)$$

Figure 6 displays the entropy change due to magnetic field (ΔS_M) as a function of temperature for the various magnetic fields. The curves showed a characteristic broad peak with a maximum in the vicinity of the magnetic transition temperature and the peak width increased as the applied magnetic field increased. The position of the maximum shifted from 43 to 45 K when the magnetic field (H) increased from 1 to 10 T. The maximum peak value of $-\Delta S_M(T)$ at each value of applied field (H) (ΔS_{Mmax}) increased linearly with increasing magnetic field up to 1.1 J mol^{-1} K^{-1} at 10 T. The field-induced magnetic transition contributed to the enhancement of magnitude of ΔS_M.

Universal curve

Then phenomenological universal curve for second-order transitions as suggested by Franco and Conde [30] converges the ΔS_M versus temperature curves to a single universal curve if ($-\Delta S_M/\Delta S_{Mmax}$) versus a reduced number (θ) is plotted with

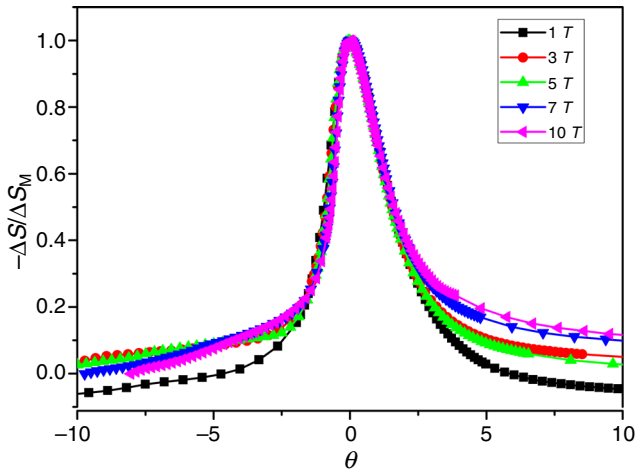

Fig. 7 The *curves* of Fig. 6 can be reduced to almost a single universal curve by following the formulism of Franco and Conde [30] using $-\Delta S_M/-\Delta S_{Mmax}$ and $\theta = (T–T_c)/(T_r–T_c)$ in the y and x axes, respectively.

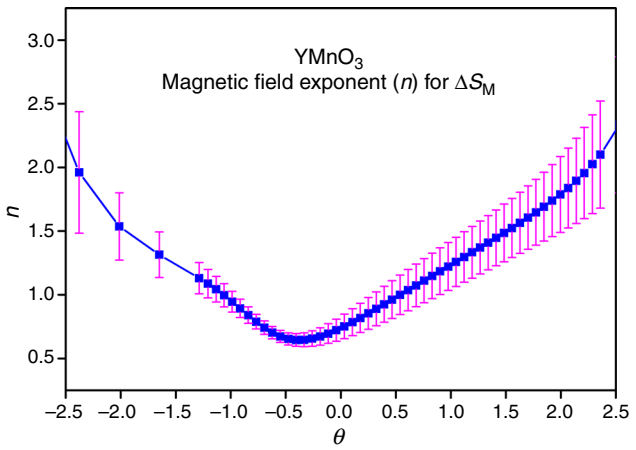

Fig. 8 Variation in magnetic field exponent (n) of $-\Delta S_M$ ($-\Delta S_M \propto H^n$) has been plotted as a function of the reduced parameter (θ). The *vertical bars* at each data point give the estimated errors in 'n'

$$\theta = (T - T_c)/(T_r - T_c), \quad (8)$$

where T_c is the temperature; ΔS_{Mmax} occurs in $-\Delta S_M$ versus T curves, and T_r is the temperature where $-\Delta S_M$ is equal to 0.7 ΔS_{Mmax} in $-\Delta S_M$ versus T curve.

Similar convergence of MCE behavior has been seen for $La_{2/3}Ba_{1/3}BaMnO3$ [31] and other compounds [32]. In the present case for $YMnO_3$, $(-\Delta S_M/\Delta S_{Mmax})$ versus the reduced number (θ) was plotted and is shown in Fig. 7. The convergence of all curves of Fig. 6 was seen in Fig. 7 due to scaling discussed above.

The magnetic field dependence of ΔS_M follows a power law [30], $\Delta S_M \propto H^n$ with the exponent being temperature dependent. From the slope of the log–log plot of $-\Delta S_M$ versus H, the exponent (n) was calculated and the plot of 'n' versus the reduced number (θ) is shown in Fig. 8. The value of 'n' varied between 0.5 and 2.0 in the θ range of −2.5 to +2.5. Within experimental errors (given as error bars in Fig. 8), the magnetic field exponent values compared well with the values (obtained by Franco and Conde [30] for alloys.

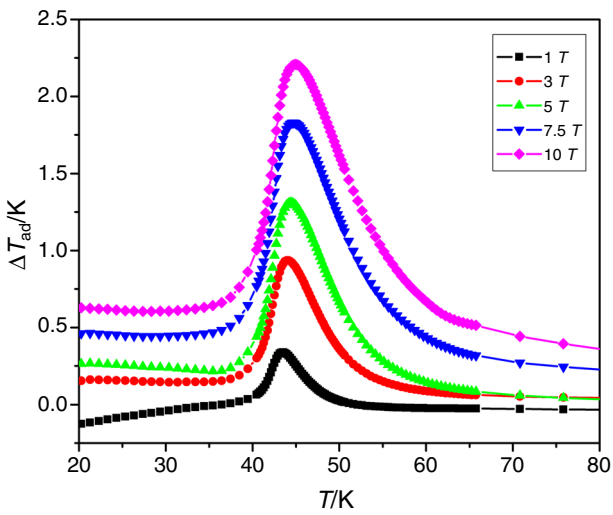

Fig. 9 The temperature (T) dependence of the adiabatic temperature difference (ΔT_{ad}) calculated from the magnetic entropy changes have been plotted for different applied magnetic fields

Relative cooling power

The adiabatic temperature difference (ΔT_{ad}) could be obtained from the isentropic difference between the entropy curves $S(0,T)$ and $S(H,T)$ [24]. The temperature dependence of ΔT_{ad} is plotted in Fig. 9 for different magnetic fields. The peak of the ΔT_{ad} versus T curve, ΔT_{admax}, occurred at a ΔT_{ad} value of 2.2 K for a magnetic field change of 10 T. In addition to the values of ΔS_{Mmax} and ΔT_{ad}, the relative cooling power (RCP) could also be evaluated to determine the cooling efficiency of a magnetocaloric material. RCP based on the magnetic cooling power is defined as the product of ΔS_{Mmax} and the full width at half maximum, δT_{FWHM}, of ΔS_M versus T curve, i.e., RCP = $\Delta S_{Mmax} \times \delta T_{FWHM}$. In Table 3, we have presented RCP values as a function of magnetic field change from 0T. RCP increased with the increase in field. The RCP value at a magnetic field change of 5T was 26 J kg^{-1}. For bulk $LaMnO_3$ and Ca or Ba substituted $LaMnO_3$, Biswas et al. [33] report an RCP value in the range of 22–250 J kg^{-1} for a magnetic field change of 5T and the value reported for $YMnO_3$ here falls within that range. Therefore, the magnetocaloric properties of $YMnO_3$ satisfies some important criteria for selecting it as a

Table 3 Variation of maximum magnetic entropy change (ΔS_{Mmax}), relative cooling power (RCP), and other relevant parameters with applied magnetic field for bulk $YMnO_3$

Field/ T	ΔS_{Mmax}/ J mol^{-1} K^{-1}	ΔT_{admax}/ K	δT_{FWHM}/ K	RCP/ J kg^{-1}
1	0.19	0.33	3.75	3.9
3	0.48	0.93	6.15	15.6
5	0.64	1.31	7.78	26.0
7.5	0.86	1.83	10.53	47.3
10	1.01	2.2	12.22	64.41

magnetic refrigerants such as exhibition of large magnetic entropy change, large adiabatic temperature change, and high RCP value.

Conclusions

Polycrystalline $YMnO_3$ multiferroic samples with hexagonal crystal structure were prepared by the solid state reaction method and the crystal structure was confirmed by XRD studies. Magnetization and specific heat measurements were carried out under different magnetic fields over a temperature range 2–300 K. The specific heat and magnetization measurements exhibited a PM to ferrimagnetic phase transition at $\sim$42 K that was also a spin glass transition. A large magnetic entropy change of $\sim$1 J mol^{-1} K^{-1} was obtained for, under, a magnetic field change of 0–10 T.

Acknowledgements The authors are grateful to DRDO, Govt. of India for supporting the present research work through a Research project (No. EPR/ER/0803750/M/01/1207). Second author thanks CSIR for providing fellowship. We also thank the Director, UGC-DAE CSR, Indore and Dr. D. Das, Dr. S. Chatterjee, and Mr. P. V. Rajesh, UGC-DAE CSR, Kolkata, Prof. R. K. Kotnala, Dr. Jyoti Shah, NPL, Delhi and Prof. D. Varshney, DAVV, Indore for their valuable discussions, encouragement, and guidance. We acknowledge the funding of DST, Government of India, for providing funds to the PPMS and MPMS facility at CSR India.

References

1. Aken BBV, Palstra TTM, Filippetti A, Spaldin NA. The origin of ferroelectricity in magnetoelectric $YMnO_3$. Nat Mater. 2004;3:164–70.
2. Fiebig M, Fröhlich D, Kohn K, Leute S, Lottermoser T, Pavlov VV, Pisarev RV. Determination of the magnetic symmetry of hexagonal manganites by second harmonic generation. Phys Rev Lett. 2000;84:5620–3.
3. Lorenz B, Litvinchuk AP, Gospodinov MM, Chu CW. Field-induced reentrant novel phase and a ferroelectric-magnetic order coupling in $HoMnO_3$. Phys Rev Lett. 2004;92:087204.
4. Alicea J, Motrunich OI, Hermele M, Fisher MPA. Criticality in quantum triangular antiferromagnets via fermionized vortices. Phys Rev B. 2005;72:064407–23.
5. Helton JS, Singh DK, Nair HS, Elizabeth S. Magnetic order of the hexagonal rare-earth manganite $Dy_{0.5}Y_{0.5}MnO_3$. Phys Rev B. 2011;84:064434–6.
6. Liu P, Wang XL, Cheng ZX, Du Y, Kimura H. Structural, dielectric, antiferromagnetic, and thermal properties of the frustrated hexagonal $Ho_{1-x}Er_xMnO_3$ manganites. Phys Rev B. 2011;83:144404–8.
7. Midya A, Khan N, Bhoi D, Mandal P. 3d-4f spin interaction induced giant magnetocaloric effect in zircon-type $DyCrO_4$ and $HoCrO_4$ compounds. Appl Phys Lett. 2013;103:092402.
8. Chatterji T, Ouladdiaf B, Henry PF, Bhattacharya D. Magnetoelastic effects in multiferroic $YMnO_3$. J Phys Condens Matter. 2012;24:336003–6.
9. Huang ZJ, Cao Y, Sun YY, Xue YY, Chu CW. Coupling between the ferroelectric and antiferromagnetic orders in $YMnO_3$. Phys Rev B. 1997;56:2623–6.
10. Gschneidner Jr KA, Pecharsky VK, Tsokol AO. Recent developments in magnetocaloric materials. Rep Prog Phys. 2005;68:1479–539.
11. Provenzano V, Li J, King T, Canavan E, Shirron P, DiPirro M, Shull RD. Enhanced magnetocaloric effects in $R_3(Ga_{1-x}Fe_x)_5O_{12}$ (R = Gd, Dy, Ho; $0 < x < 1$) nanocomposites. J Magn Magn Mater. 2003;266:185–93.
12. Eerenstein W, Mathur ND, Scott JF. Multiferroic and magnetoelectric materials. Nature. 2006;442(7104):759–65.
13. Cheong SW, Mostovoy M. Multiferroics: a magnetic twist for ferroelectricity. Nat mater. 2007;6(1):13–20.
14. Fiebig M. Revival of the magnetoelectric effect. J Phys D Appl Phys. 2005;38(8):R123–52.
15. Chen WR, Zhang FC, Miao J, Xu B, Dong XL, Cao LX, Qiu XG, Zhao BR. Re-entrant spin glass behavior in Mn-rich $YMnO_3$. Appl Phys Lett. 2005;87(042508):1–3.
16. Koehler WC, Yakel HL, Wollan EO, Cable JW. A note on the magnetic structures of rare earth manganese oxides. Phys Lett. 1964;9(2):93–5.
17. Karche BR, Khasbardar BV, Vaingankar AS. X-ray, SEM and magnetic properties of Mg-Cd ferrites. J Magn Magn Mater. 1997;168:292–8.
18. Smit J, Wijin HPJ. Ferrites. 1st ed. New York: Wiley; 1959.
19. Smit J. Magnetic properties of materials. New York: McGraw-Hill; 1971. p. 89.
20. Khan MHR, Hossain AKMA. Reentrant spin glass behavior and large initial permeability of $Co_{0.5-x}Mn_xZn_{0.5}Fe_2O_4$. J Magn Magn Mater. 2012;324:550–8.
21. Kimura T, Ishihara S, Shintani H, Arima T, Takahashi KT, Ishizaka K, Tokura Y. Distorted perovskite with e_g^1 configuration as a frustrated spin system. Phys Rev B. 2003;68(060403(R)):1–4.
22. Kumar NP, Lalitha G, Reddy PV. Specific heat and magnetization studies of $RMnO_3$ (R = Sm, Eu, Gd, Tb and Dy) multiferroics. Phys Scr. 2011;83(045701):1–8.
23. Tomuta DG, Ramakrishnan S, Nieuwenhuys GJ, Mydosh JA. The magnetic susceptibility, specific heat and dielectric constant of hexagonal $YMnO_3$, $LuMnO_3$ and $ScMnO_3$. J Phys Condens Matter. 2001;13:4543–52.
24. Pecharsky VK, Gschneidner JKA. Giant Magnetocaloric Effect in $Gd_5(Si_2Ge_2)$. Phys Rev Lett. 1997;78(23):4494–7.
25. Korolev VV, Arefyev IM, Ramazanova AG. The magnetocaloric effect of superfine magnets. J Therm Anal Calorim. 2008;92(3):691–5.
26. Cheng JG, Sui Y, Wang XJ, Liu ZG, Miao JP, Huang XQ, Lu Z, Qian ZN, Su WH. Specific heat of single-crystal $PrMnO_3$. J Phys Condens Matter. 2005;17:5869–79.
27. Hamad Mahmoud A. Magnetocaloric properties of $La_{0.6}Ca_{0.4}MnO_3$. J Therm Anal Calorim. 2013;113(2):609–13.

28. Hamad Mahmoud A. Magnetocaloric effect in $La_{1.25}Sr_{0.75}MnCoO_6$. J Therm Anal Calorim. 2014;115(1):523–6.
29. Tishin AM, Spichkin YI. The Magnetocaloric effect and its applications. London: Institute of Physics Publishing; 2003.
30. Franco V, Conde A. Scaling laws for the magnetocaloric effect in second order phase transitions: from physics to applications for the characterization of materials International. J Refrig. 2010;33:465–73.
31. M'nassri R, Cheikhrouhou A. Evolution of Magnetocaloric Behavior in Oxygen Deficient $La_{2/3}Ba_{1/3}MnO_{3-\delta}$ Manganites. J Supercond Novel Magn. 2014;27:1463–8.
32. M'nassri R. Field dependence of magnetocaloric properties in $La_{0.6}Pr_{0.4}Fe_{10.7}Co_{0.8}Si_{1.5}$. J Supercond Novel Magn. 2014;27:1787–94.
33. Biswas A, Chandra S, Phan Manh-Huong, Srikanth H. Magnetocaloric properties of nanocrystalline $LaMnO_3$: enhancement of refrigerant capacity and relative cooling power. J Alloy Compd. 2012;545:157–61.